Parts, Ü.; Karimäki, J.; Koivuniemi, J.; Krusius, M.; Ruutu, V.; Thuneberg, E.; Volovik, G.

Phase diagram of vortices in superfluid 3He-A

Published in:
Physical Review Letters

DOI:
10.1103/PhysRevLett.75.3320

Published: 01/01/1995

Document Version
Publisher's PDF, also known as Version of record

Please cite the original version:
Parts, Ü., Karimäki, J., Koivuniemi, J., Krusius, M., Ruutu, V., Thuneberg, E., & Volovik, G. (1995). Phase diagram of vortices in superfluid 3He-A. *Physical Review Letters*, *75*(18), 3320-3323. https://doi.org/10.1103/PhysRevLett.75.3320

Phase Diagram of Vortices in Superfluid ^{3}He-A

Ü. Parts, J. M. Karimäki, J. H. Koivuniemi, M. Krusius, V. M. H. Ruutu, E. V. Thuneberg, and G. E. Volovik*
Low Temperature Laboratory, Helsinki University of Technology, 02150 Espoo, Finland
(Received 6 June 1995)

Four alternative but topologically different structures of vorticity exist in rotating ^{3}He-A. As a function of magnetic field (H) and rotation velocity (Ω), we identify with NMR the type of vortex which is nucleated during cooling from the normal to the superfluid phase. The measurements are compared to the calculated equilibrium phase diagram of vortices in the H-Ω plane at temperatures $T \lesssim T_c$. Slow transitions are found to reproduce the calculated equilibrium state.

PACS numbers: 67.57.Fg, 05.70.Fh

Soon after the discovery of the superfluid phases of liquid ^{3}He it became evident that the anisotropic A phase could support unusual types of vorticity [1,2]. In different rotating experiments, four alternative structures have been identified with various measuring techniques [3–6]. We describe here the first measurements in which all four vortex types can be created and detected in the same experiment. This allows us to measure their phase diagram by cooling slowly into the superfluid phase in a rotating container at constant rotation and magnetic field. The experimental result is found to agree with our numerically computed equilibrium phase diagram. The underlying principles are of interest for a discussion of the dimensionality and structure of topological defects formed in a symmetry-breaking phase transition. Superfluid phases of ^{3}He, with their many competing defects, can be used as a laboratory model which may help us to understand, for instance, the nucleation of cosmic strings in the early universe [7]. This is especially true for the A phase, which has many similarities with the vacuum of electroweak interactions [8].

Superfluid ^{3}He-A.—The superfluid state of ^{3}He-A is described by a 3×3 matrix order parameter $A_{\alpha k} = \Delta \hat{d}_\alpha (\hat{m}_k + i\hat{n}_k)$ [9]. The unit vector $\hat{\mathbf{d}}$ denotes a symmetry-breaking direction in the spin space. The orthogonal unit vectors $\hat{\mathbf{m}}$ and $\hat{\mathbf{n}}$ define the direction of the orbital angular momentum $\hat{\mathbf{l}} = \hat{\mathbf{m}} \times \hat{\mathbf{n}}$, which is analogous to the direction of the isotopic spin in the electroweak vacuum.

The superfluid velocity is generally defined as the gradient of the phase ϕ: $\mathbf{v}_s = (\kappa/2\pi)\nabla\phi$. (Here κ is the circulation quantum, equal to Planck's constant divided by twice the mass of an atom in ^{3}He.) In ^{3}He-A, a phase factor $\exp(i\phi)$ is equivalent to a rotation of $\hat{\mathbf{m}}$ and $\hat{\mathbf{n}}$ around $\hat{\mathbf{l}}$, so that this definition has to be generalized to $\mathbf{v}_s = (\kappa/2\pi)\hat{m}_i \nabla \hat{n}_i$. It follows that instead of being potential, $\mathbf{v}_s$ has nonzero circulation which depends on the orientational distribution of $\hat{\mathbf{l}}(\mathbf{r})$ [1],

$$\oint d\mathbf{r} \cdot \mathbf{v}_s = \frac{\kappa}{2\pi} \int dx\, dy \hat{\mathbf{l}} \cdot (\partial_x \hat{\mathbf{l}} \times \partial_y \hat{\mathbf{l}}) . \qquad (1)$$

Here the vorticity is assumed parallel to z, i.e., $\hat{\mathbf{l}}(\mathbf{r}) = \hat{\mathbf{l}}(x, y)$. The integral on the right equals the net area which $\hat{\mathbf{l}}(\mathbf{r})$ sweeps of the surface of a unit sphere $\hat{\mathbf{l}} \cdot \hat{\mathbf{l}} = 1$.

The degeneracy of the order-parameter manifold is reduced by two interactions. The dipole-dipole interaction leads to the energy $f_d = -\frac{1}{2} g_d (\hat{\mathbf{d}} \cdot \hat{\mathbf{l}})^2$, and an external magnetic field $\mathbf{H}$ produces $f_H = \frac{1}{2} g_H (\hat{\mathbf{d}} \cdot \mathbf{H})^2$. In the absence of frustration, f_H fixes $\hat{\mathbf{d}}$ perpendicular to $\mathbf{H}$, while f_d forces a "locked" configuration with $\hat{\mathbf{l}} = \pm\hat{\mathbf{d}}$.

Vortex structures.—Neglecting boundary effects, the equilibrium state of rotating ^{3}He-A has a periodic pattern of vorticity. The different vortex structures can be classified with a few quantum numbers, which characterize one unit cell of the two-dimensional Bravais lattice. The circulation number is defined by $N = \oint d\mathbf{r} \cdot \mathbf{v}_s/\kappa$. The vortices can be either singular or continuous. The latter alternative means that the order parameter retains the A-phase form everywhere. For continuous vortices we can further define the winding numbers ν_l and ν_d from the integral $\nu_l = (1/4\pi) \int dx\, dy \hat{\mathbf{l}} \cdot (\partial_x \hat{\mathbf{l}} \times \partial_y \hat{\mathbf{l}})$ and its analog for the $\hat{\mathbf{d}}$ field. It follows from Eq. (1) that $N = 2\nu_l$; i.e., the circulation is simply related to the area $\hat{\mathbf{l}}$ sweeps on the surface of the unit sphere.

The $\hat{\mathbf{l}}(\mathbf{r})$ fields of the four vortex types are shown in Fig. 1. (i) The first vortex, which was observed in NMR measurements [3], is the continuous unlocked vortex (CUV) with quantum numbers $N = 2\nu_l = 2$ and $\nu_d = 0$ [10]. The unlocked region, the "soft" core, where $\hat{\mathbf{l}} \neq \pm\hat{\mathbf{d}}$, is shown shaded in Fig. 1.

(ii) The singular vortex (SV) has been experimentally a controversial object. In this measurement it is reliably identified for the first time, but in retrospect we can ascribe part of the earlier data from ion transmission measurements [4,11] to the SV. Although it is not required by topology, the SV has for energetic reasons also a soft core with a nonuniform $\hat{\mathbf{l}}$ texture ($\nu_l \approx 1/2$ and $\nu_d \approx 0$) [10]. The hard core, where $\hat{\mathbf{l}}$ is not defined, is displaced from the center of the vortex. In spite of a large energy contribution from the hard core, the singular vortex is favored at low angular velocity Ω since it has the smallest circulation with $N = 1$.

(iii) The locked vortex (LV) has topologically equivalent $\hat{\mathbf{l}}$ and $\hat{\mathbf{d}}$ fields, i.e., $\nu_l = \nu_d = N/2$. The first experimental indication comes from ultrasound absorption measurements [5]. This structure is favored in low magnetic fields where the cost of $\hat{\mathbf{d}}$ not being perpendicular to

 0031-9007/95/75(18)/3320(4)$06.00

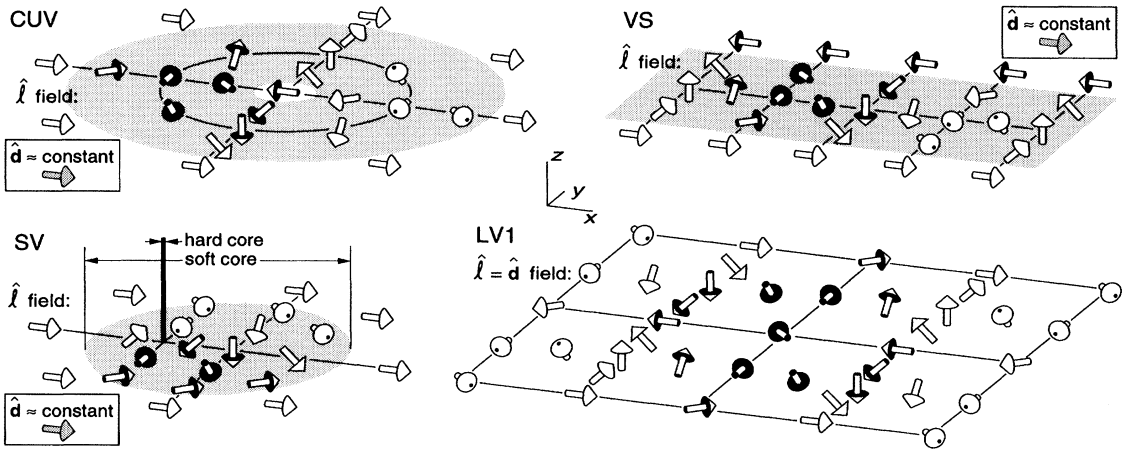

FIG. 1. Four vortex structures of rotating ^{3}He-A: continuous unlocked vortex (CUV), vortex sheet (VS), singular vortex (SV), and locked vortex (LV1). The arrows denote the orientation of $\hat{\mathbf{l}}$ in the x-y plane. The rotation axis $\mathbf{\Omega}$ is parallel to z. The shaded area marks the "soft core" of the unlocked vortices (CUV, VS, and SV) where $\hat{\mathbf{d}}$ and $\hat{\mathbf{l}}$ deviate from each other. In the LV, $\hat{\mathbf{d}}$ and $\hat{\mathbf{l}}$ follow each other everywhere. The $\hat{\mathbf{l}}$ field is continuous with the exception of the SV, where $\hat{\mathbf{l}}$ is not defined in the "hard core." In all cases the vorticity has periodicity in the x-y plane, but the complete periodic unit is depicted for the LV1 only. For the VS one full periodic unit in the x direction is shown; by stacking these units one after another, its soft core becomes a continuous sheet. The CUV is equivalent to one period of the VS, when it is bent and closed to a cylinder. The length scales are 0.01 and 10 μm for the hard and soft cores, respectively, and 200 μm (at $\Omega = 1$ rads/s) for the unit cell.

$\mathbf{H}$ is not serious. Two lattice structures have been predicted for the LV. One of them has a circulation number $N = 4$ and a square lattice (LV1, Fig. 1) [12], while the other has $N = 2$ and a stretched triangular lattice (LV2, not shown in Fig. 1) [13].

(iv) Finally, the vortex sheet (VS), first identified in NMR measurements [6], has the same quantum numbers as the CUV. The difference between the two becomes evident when their periodic units are stacked one after another: the CUV forms a lattice of vortex lines while the VS forms a series of equidistant soliton planes.

Experiment.—The vortices are nucleated at fixed Ω and H by cooling from the normal phase, through the superfluid transition temperature T_c, to some final temperature T_f well below T_c. During this process the vortex state evolved at some $T \lesssim T_c$ will freeze in because transitions between vortex types become suppressed at low temperatures. If T_f is sufficiently low, then no transitions take place even if the field is changed at T_f. Thus, the superfluid transition can be traversed at different fields, and the NMR measurement is done independently at a lower temperature with the field at the NMR value H_{NMR}.

The measurements were performed in a rotating cryostat. Two improvements were important: (1) The measuring technique was transverse continuous wave NMR at a fixed frequency with a linear field sweep around the Larmor field $H_{\mathrm{NMR}} \approx 11$ mT. The measuring sensitivity was much enhanced with a superconducting high-Q resonance circuit connected directly to a preamplifier operating at 4.2 K. (2) Supercooling of ^{3}He-A was necessary to suppress the transition LV $\rightarrow$ CUV. It also greatly improved the frequency resolution of the NMR peaks. Supercooling depends on the smoothness of the sample cell walls [14]. Two cylinders were used, one made of epoxy and the other of fused quartz. In the latter, the smooth walls allowed ^{3}He-A to be cooled to $0.45T_c$ at 34.2 bars, while the thermodynamic $T_{AB} = 0.78T_c$. The ^{3}He containers had a radius of 2.5 mm, a height of 7 mm, and both $\mathbf{H}$ and $\mathbf{\Omega}$ were aligned along the axis of the cylinder.

Identification of vortex structures.—Four NMR absorption spectra are shown in Fig. 2. Each spectrum has a main peak and one or more satellite peaks. Only the main peak is present in the nonrotating equilibrium state ($\hat{\mathbf{l}} = \pm\hat{\mathbf{d}} \perp \mathbf{H}$). The satellite peaks arise from vortices in the rotating state. The different vortex types can be distinguished from the frequencies and intensities of the satellites. The spectra from the CUV and VS in Fig. 2 have been described previously [3,6]. Here we concentrate on the SV and LV, which have not been seen with NMR before.

The frequency shifts of the satellites are independent of Ω. For satellites that arise from vortex lines, the intensity is proportional to Ω, or the number of lines in the equilibrium state. The reason is that (at H_{NMR} and $\Omega \lesssim 3$ rad/s) the vortices are far apart and respond independently to NMR. The identification of the SV spectrum is justified by the following considerations: (1) The spectrum clearly differs from that of the CUV and VS. (2) The frequency and intensity of the satellite peak are in quantitative agreement with model calculations on the SV [10]. The frequency ν agrees with the one calculated by Vulovic *et al.* with accuracy $0.01\Delta\nu_{\mathrm{main}}$ at $T = 0.8T_c$ and $0.05\Delta\nu_{\mathrm{main}}$ at $T = 0.7T_c$. The intensity agrees within 30%. (3) The spectrum is recorded under the conditions where the SV is expected to appear (Fig. 3).

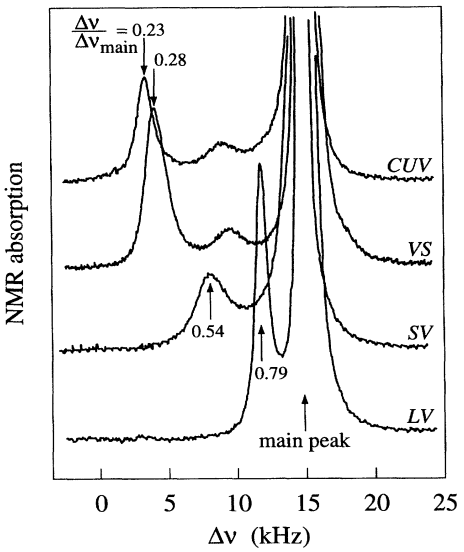

FIG. 2. Four NMR absorption spectra measured in rotating supercooled ^{3}He-A. The horizontal axis is the frequency shift from the Larmor value $\gamma H_{\rm NMR}$. The shift of the main peak is used for thermometry. Each spectrum is labeled with the vortex type that gives rise to one or two visible satellite peaks. The measuring conditions at 34.2 bars pressure are essentially the same for all spectra (CUV)-(LV) Ω(rad/s) = 0.58, 0.7, 0.58, 0.4, and T/T_c = 0.49, 0.50, 0.52, 0.49, respectively.

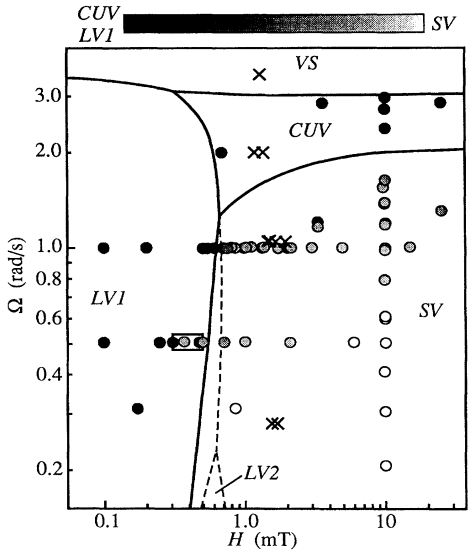

FIG. 3. Phase diagram of vortices in the magnetic field H and rotation velocity Ω plane. Each circle represents a rotational state created by cooling through T_c at constant H and Ω, under 29.3 bars pressure. The shading of the circles indicates the relative number of continuous vortices. The SV (open circles) dominates when $H > 1$ mT and $\Omega < 2$ rad/s, while continuous vortices (filled circles) occupy two regions (LV1 and CUV). The transition between the LV1 and SV agrees with an earlier measurement (rectangle) [4] where vortices were created in a similar manner but detected with ion transmission. The crosses mark transitions between the CUV and LV1 from an experiment where vortices were created by increasing Ω at a constant $T \approx 0.9T_c$, and detected by ultrasound [5]. The lines denote the theoretical phase diagram where the LV2 appears only as metastable (dashed lines) within the stable region of the SV. We have used the parameter values $\Omega_d = 2mg_d/\hbar\rho_\parallel = 180$ rad/s [$\xi_d = (\hbar/2m)\sqrt{\rho_\parallel/g_d} = 7.6\,\mu$m], and $H_d = \sqrt{g_d/g_H} = 2.0$ mT, where $\rho_\parallel$ is the superfluid density parallel to $\hat{\mathbf{l}}$. For clarity of the figure, the former was chosen larger than our independent estimate $\Omega_d \approx 120$ rad/s.

The LV spectrum is obtained if the field is kept low until the temperature has been reduced below $0.6T_c$, after which H is increased to the measuring value $H_{\rm NMR}$. This spectrum has a large satellite that is only slightly displaced from the main peak. We associate the satellite with the LV which, in the measuring situation, is distorted by the large field $H_{\rm NMR}$. The justification is as follows: (1) The satellite differs from those of the other vortices by its frequency and intensity. (2) The vortex state is created in low field, where the LV prevails. (3) Only a small frequency displacement from the main peak is expected because a structure with $\hat{\mathbf{l}} \equiv \pm\hat{\mathbf{d}}$ should give no shift.

Experimental phase diagram.—The results of the measurements are shown in Fig. 3. After each cool-down from the normal phase with constant H and Ω, the number of vortices of different type was determined from the satellite peaks. The general features of the phase diagram are as expected: The SV occupies the region of high H and low Ω. If the field is reduced, then the LV is obtained, or, if Ω is increased, then the CUV prevails.

Some more detailed observations are also in order: (1) The VS can be created in a few different ways below T_c [6], but it did not show up by simply cooling through T_c. Apparently, our maximum $\Omega = 3$ rad/s is too low for the VS to appear (see below). (2) The phase transitions between different vortex types are broadened. In each case there seems to be an overlap regime where two different types of vortices are simultaneously present such that there is a smooth change in their relative number on crossing the coexistence regime. (3) The transition between the LV and CUV was not studied in detail because our test runs agree with earlier results [5] although these have been measured under somewhat different conditions.

The broadening of the phase transitions in Fig. 3 is related to the details of how nucleation proceeds at T_c. Large cooling rates are observed to increase the ratio of continuous versus singular vortices. The data in Fig. 3 have been collected at cooling rates $\leq 5\ \mu$K/min, when the dependence on the rate starts to wear out. A further complication is that in a magnetic field the superfluid transition is split into A_1 and A_2 phases so that $T_{A1} - T_{A2} = (0.6\ \mu\text{K})H/(10\ \text{mT})$. Moreover, the container has a thermal gradient, which means that a second-order phase transition proceeds in the form of a phase front similar to a first-order transition. The discussion of the transition details is deferred to a later report.

Generally, rotating experiments on ^{3}He-A were done by first cooling to the superfluid state and only then starting the rotation. If the temperature is sufficiently close to T_c (i.e., $1 - T/T_c < 2 \times 10^{-3}$), we find that accelerating rotation at constant T seems to yield the same result as in Fig. 3. However, at any lower temperature only continuous vortices are formed. The evident reason is that the hard core of a SV has a high energy density, and is not easily nucleated out of a uniform flow field, even though the total energy would be smaller for a SV than for a continuous vortex. In fact, the energy barriers between different vortex types become so large at low T that no transitions take place. We see no decay in states consisting of CUV or SV at $T < 0.99T_c$, irrespective of H, and the same holds for the VS if $T < 0.90T_c$ and $H > 1$ mT [6]. The easiest transition is that from LV to CUV, which (at $H \lesssim 10$ mT) is suppressed only below $0.6T_c$. There seems to be no practical way of determining the general phase diagram at temperatures far below T_c.

Theoretical phase diagram.—The equilibrium vortex structure can be calculated by minimizing the free energy. For continuous vortices the functional consists of the external field energy f_H, dipole-dipole energy f_d, kinetic energy, and gradient energies for $\hat{\mathbf{d}}$ and $\hat{\mathbf{l}}$ [9]. We have constructed a computer program that minimizes this functional for vortices close to T_c, but we exclude the region nearest to T_c, where the A phase is distorted toward the A_1 phase. Initially, a periodic guess for the $\hat{\mathbf{l}} = \hat{\mathbf{m}} \times \hat{\mathbf{n}}$ and $\hat{\mathbf{d}}$ fields is made. Then the fields are iteratively changed toward a minimum of energy without imposing any constraints other than the initial periodicity. We have found the four different continuous structures (LV1, LV2, CUV, and VS) by trying out a number of different initial guesses. The phase boundaries between them are marked in Fig. 3.

The singular vortex was not initially included in the calculation because its two very different length scales (for the hard and soft core radii) make this difficult. However, it was approximately incorporated in the phase diagram by assuming the core energy to be a constant, independent of H and Ω. The constant was determined by fitting to the experimental data. Besides some uncertainty in the scaling factors of the Ω and H axes, this constant is the only adjustable parameter in the theoretical phase diagram.

Some separate pieces of the phase diagram have been calculated before, using variational models [10,13]. A qualitatively new feature in the diagram is the vortex sheet, which seems to form the equilibrium state at surprisingly low Ω. Another unexpected result is that both the VS and CUV become favored over the LV at large Ω, even in zero field [15]. We understand this so that the LV has gradient energy associated with the $\hat{\mathbf{d}}$ field, and with increasing Ω it becomes more costly than the energy associated with the soft core in the VS and CUV.

In conclusion, on comparing the experimental and theoretical phase diagrams, we see that they are in qualitative agreement. This is not entirely obvious since the calculation addresses the equilibrium state in the A phase, but the experiment involves the dynamical process of vortex nucleation. Indeed, the dependence on the cool-down rate and the complexities of the transition into the superfluid state let us anticipate that the opposite limit of rapidly quenched transitions is an important direction to pursue [16]. What also remains for future experiments is the verification of the vortex-sheet ground state at large rotation velocities, and the distinction of the two types of locked vortices.

*Permanent address: L.D. Landau Institute for Theoretical Physics, 117334 Moscow, Russia.

[1] N. D. Mermin and T.-L. Ho, Phys. Rev. Lett. **36**, 594 (1976); T.-L. Ho, Phys. Rev. B **18**, 1144 (1978).
[2] V. R. Chechetkin, Zh. Eksp. Teor. Fiz. **71**, 1463 (1976) [Sov. Phys. JETP **44**, 766 (1976)]; P. W. Anderson and G. Toulouse, Phys. Rev. Lett. **38**, 508 (1977).
[3] P. J. Hakonen, O. T. Ikkala, and S. T. Islander, Phys. Rev. Lett. **49**, 1258 (1982); P. Hakonen, M. Krusius, and H. Seppälä, J. Low Temp. Phys. **60**, 187 (1985).
[4] J. Simola, L. Skrebek, K. Nummila, and J. Korhonen, Phys. Rev. Lett. **58**, 904 (1987); J. Low Temp. Phys. **75**, 111 (1989).
[5] J. P. Pekola, K. Torizuka, A. J. Manninen, J. M. Kyynäräinen, and G. E. Volovik, Phys. Rev. Lett. **65**, 3293 (1990); **67**, 1055 (1991).
[6] Ü. Parts, E. V. Thuneberg, G. E. Volovik, J. H. Koivuniemi, V. M. H. Ruutu, M. Heinilä, J. M. Karimäki, and M. Krusius, Phys. Rev. Lett. **72**, 3839 (1994); three articles in Physica (Amsterdam) **210B**, 287-333 (1995).
[7] M. B. Hindmarsh and T. W. B. Kibble, Rep. Prog. Phys. **58**, 477 (1995).
[8] T. Vachaspati and G. E. Volovik (to be published).
[9] D. Vollhardt and P. Wölfle, *The Superfluid Phases of ^{3}He* (Taylor & Francis, London, 1990).
[10] H. Seppälä and G. Volovik, J. Low Temp. Phys. **51**, 279 (1983); V. Vulovic, D. Stein, and A. Fetter, Phys. Rev. B **29**, 6090 (1984); A. Fetter, J. Low Temp. Phys. **67**, 145 (1987).
[11] Only one type of singular vortex has been observed; it differs from that expected at very high Ω [15].
[12] T. Fujita, M. Nakahara, T. Ohmi, and T. Tsuneto, Prog. Theor. Phys. **60**, 671 (1978).
[13] X. Zotos and K. Maki, Phys. Rev. B **31**, 7120 (1985).
[14] P. Schiffer, M. T. O'Keefe, M. D. Hildreth, H. Fukuyama, and D. D. Osheroff, Phys. Rev. Lett. **69**, 120 (1992).
[15] A. L. Fetter, J. A. Sauls, and D. L. Stein, Phys. Rev. B **28**, 5061 (1983).
[16] P. C. Hendry, N. S. Lawson, R. A. M. Lee, P. V. E. McClintock, and C. D. H. Williams, Nature (London) **368**, 315 (1994).